ISSN 1070-3284, Russian Journal of Coordination Chemistry, 2016, Vol. 42, No. 5, pp. 316–323. © Pleiades Publishing, Ltd., 2016.

Ln(III) Metal-Organic Frameworks with 5-Nitroisophthalate Ligands: Crystal Structures and Luminescent Properties[1]

J. J. Wang*, Y. J. Zhang, F. Jin, E. N. Wang, M. Y. Zhang, and J. Chen

College of Chemistry and Chemical Engineering, Anyang Normal University, Anyang, Henan, 455000 P.R. China

**e-mail: jjwang@aynu.edu.cn*

Received May 19, 2015

Abstract—Two new Ln(III) metal-organic frameworks (MOFs) based on 5-nitroisophthalic acid (H_2L), namely $[Pr_4(L)_6(H_2O)_4]_n$ (**I**) and $[Gd(L)(FA)(H_2O)_2]_n$ (**II**) (HFA = formic acid), were prepared by solvothermal reactions and structurally characterized by IR, elemental analysis, XRD, and single crystal X-ray diffraction (CIF files CCDC nos. 971379 (**I**) and 971380 (**II**)). A 3D $\{4.6^2\}\{4^{10}.6^{17}.8^9\}\{4^3\}_2$ topology framework of **I** and a 3D $\{4.6^2\}_2\{4^2.6^{10}.8^3\}$ topology network of **II** are constructed respectively with different synthetic conditions. Four kinds of coordination modes are observed for dicarboxylate in these two MOFs in total. Notably, the in situ hydrolysis of DMF solvates leads to the formation of formate ions that was observed in the structure of **II**. Moreover, the luminescent properties of both complexes and corresponding ligand have been investigated.

DOI: 10.1134/S1070328416050080

INTRODUCTION

In the past decades, metal-organic frameworks (MOFs) have continuously been the subject of great interests to inorganic chemists, due to their potential applications in optics, magnetism, gas storage, ion exchange, and catalysis etc. [1]. Although much progress has been made in the construction of MOFs to date [2], effective control of the assembly architecture of MOF materials, which is vital to its application perspective, still remains great challenge in crystal engineering.

Rational utilization of ligands has been proved to be an effective strategy to control the multi-dimensional structure of MOFs varying from one- to three-dimension, the size of pores and channels of MOFs [3], as well as the properties and functions of target MOFs [4]. Among various ligands, the carboxylic acid-based ligands, especially aromatic carboxylic acids, have been widely used and well-documented in the preparations of metal-organic complexes with diverse coordination modes [5–7]. Aromatic backbones, including benzene, naphthalene and anthracene are of interest in the development of fluorescent material and are used as model compounds for electroluminescence [8], chemosensors [9] and photoinduced electron transfer sensors [10]. Introduction of these aromatic backbones will enrich the properties and application aspects of target MOFs.

Differing from transition-metal ions, rare earth ions often display variably high coordination number (typically from 7 to 10) and flexible coordination geometry, which enriches the assembly structure of MOFs, but on the other hand, makes it difficult to control the assembly.

Considering all the aspects stated above, our idea in this work is to study the complexity of assembly occurring between rare earth ions and aromatic dicarboxylate, in order to further study on assembly process of rare earth ions-based MOFs and their luminescence properties. Here, 5-nitroisophthalic acid (H_2L) [11] was chosen to synthesize two Ln(III) complexes, namely $[Pr_4(L)_6(H_2O)_4]_n$ (**I**) and $[Gd(L)(FA)(H_2O)_2]_n$ (**II**) (HFA = formic acid). Meanwhile, photoluminescence of these two complexes was observed and briefly analyzed.

EXPERIMENTAL

Materials and methods. All reagents and solvents for synthesis were commercially available and used as received or purified by standard methods prior to use. Elemental analyses (C, H and N) were performed on a Perkin-Elemer 240C analyzer. The IR spectra were recorded in the range of 4000–400 cm^{-1} on a Tensor 27 OPUS (Bruker) FT-IR spectrometer with KBr pellets. Emission spectra in solid state at room temperature were recorded on a Cary Eclips fluorescence spectrophotometer.

Synthesis of I. A mixture of H_2L (106 mg, 0.50 mmol) and $Pr(NO_3)_3 \cdot 6H_2O$ (109 mg, 0.25 mmol) was dissolved in 6 mL aqueous solution.

[1] The article is published in the original.

Table 1. Crystallographic data and structure refinement summary for complexes **I**, **II**

Parameter	Value	
	I	**II**
Formula weight	1890.39	447.41
Crystal system	Triclinic	Monoclinic
Space group	$P\bar{1}$	$P2_1/c$
a, Å	10.435(2)	10.077(2)
b, Å	16.987(3)	11.925(2)
c, Å	19.496(4)	10.387(2)
α, deg	64.50(3)	90
β, deg	81.59(3)	91.25(3)
γ, deg	76.17(3)	90
V, Å^3	3025.1(10)	1247.9(4)
Z	2	4
ρ_{calcd}, g cm^{-3}	2.075	2.381
$F(000)$	1824	852
μ, mm^{-1}	3.278	5.370
Collected reflections	28594	10964
Unique reflections	14985	3102
R_{int}	0.0165	0.0177
GOOF	0.914	1.013
R_1 ($I > 2\sigma(I)$)*	0.0226	0.0184
wR_2 (all data)**	0.0578	0.0505
$\Delta\rho_{max/\Delta}\rho_{min}$, e Å^{-3}	1.076/−1.308	0.594/−1.187

* $R = \Sigma\|\|F_o| - |F_c\|/\Sigma|F_o|$. ** $R_w = [\Sigma[w(F_o^2 - F_c^2)^2]/\Sigma w(F_o^2)^2]^{1/2}$.

The resultant solution was sealed in a 25 mL Teflon-lined stainless autoclave and heated to 160°C. After keeping in these conditions for 3 days, light green single crystals suitable for X-ray analysis were obtained after cooling to room temperature. The yield was ~40% based on H_2L (64 mg).

IR (KBr; ν, cm^{-1}): 3447 s, br, 2361 m, 2344 m, 1869 w, 1618 s, 1541 s, 1465 s, 1389 s, 1205 w, 1084 m, 1009 w, 925 w, 862 w, 789 m, 735 s, 709 m, 536 m, 452 m, 422 m.

For $C_{48}H_{26}N_6O_{40}Pr_4$

anal. calcd., %:	C, 30.48;	H, 1.39;	N, 4.45.
Found, %:	C, 30.65;	H, 1.47;	N, 4.21.

Synthesis of II. A mixture of H_2L (106 mg, 0.50 mmol) and $Gd(NO_3)_3 \cdot 6H_2O$ (113 mg, 0.25 mmol) was dissolved in 2 mL DMF and 4 mL aqueous solution. The resultant solution was sealed in a 25 mL Teflon-lined stainless autoclave and heated to 160°C. After keeping in these conditions for 3 days, light yellow single crystals suitable for X-ray analysis were obtained after cooling to room temperature. The yield was ~20% based on H_2L (45 mg).

IR (KBr; ν, cm^{-1}): 3313 s, br, 2361 m, 1869 w, 1611 s, 1559 s, 1461 m, 1417 m, 1379 s, 1344 s, 1199 m, 1098 m, 927 m, 869 w, 790 m, 737 s, 673 m, 546 m, 458 w, 419 w.

For $C_9H_8NO_{10}Gd$

anal. calcd., %:	C, 24.11;	H, 1.80;	N, 3.13.
Found, %:	C, 24.36;	H, 1.57;	N, 3.42.

XRPD patterns of I, II were recorded at 293 K on a Rigaku D/Max-2500 diffractometer, operated at 40 kV and 100 mA, using a Cu-target tube and a graphite monochromator. The crushed single-crystalline powder samples were prepared by crushing the crystals and the intensity data were recorded by continuous scan in the 2θ/θ mode from 5° to 40° with a step size of 0.02° and a scan speed of 8° min^{-1}. Simulation of the XRPD spectra was carried out by the single-crystal data and diffraction-crystal module of the Mercury (Hg) program available free of charge via the internet at http://www.iucr.org.

X-ray crystallography. Single-crystal X-ray studies for complexes **I**, **II** were performed on a Bruker APEX II CCD diffractometer at 293(2). The determinations of unit cell parameters and data collections were performed with MoK_α radiation with radiation wavelength of 0.71073 Å by using the ω-scan technique. The program SAINT [12] was used for the integration of the diffraction profiles. Semi-empirical absorption corrections were applied using the SADABS program [13]. All the structures were solved by direct methods using the SHELXS program of the SHELXTL package and refined with SHELXL [14]. Metal atoms in each complex were located from the E-maps, and other non-hydrogen atoms were located in successive difference Fourier syntheses and refined with anisotropic thermal parameters on F^2. The hydrogen atoms were added theoretically, riding on the concerned atoms and refined with fixed thermal factors. The data of **I** corroborated well with the SQUEEZE calculations [15]. Crystallographic data and experimental details for structural analyses are summarized in Table 1. Selected bond distances are listed in Table 2.

Supplementary material for structures **I**, **II** has been deposited with the Cambridge Crystallographic Data Centre (nos. 971379 and 971380, respectively; deposit@ccdc.cam.ac.uk or http://www.ccdc.cam.ac.uk).

Table 2. Selected bond distances (Å) for **I**, **II***

Bond	*d*, Å	Bond	*d*, Å
		I	
Pr(1)–O(25)	2.3793(19)	Pr(1)–O(7)	2.394(2)
Pr(1)–O(21)$^{\#1}$	2.408(2)	Pr(1)–O(13)	2.4466(19)
Pr(1)–O(19)	2.458(2)	Pr(1)–O(1*w*)	2.498(2)
Pr(1)–O(2)	2.599(2)	Pr(1)–O(1)	2.6299(18)
Pr(2)–O(16)$^{\#2}$	2.350(2)	Pr(2)–O(33)$^{\#3}$	2.372(2)
Pr(2)–O(3)	2.4179(19)	Pr(2)–O(31)	2.438(2)
Pr(2)–O(10)$^{\#2}$	2.468(2)	Pr(2)–O(2*w*)	2.532(3)
Pr(2)–O(27)$^{\#4}$	2.573(2)	Pr(2)–O(28)$^{\#4}$	2.7155(19)
Pr(3)–O(15)$^{\#5}$	2.3727(19)	Pr(3)–O(4)$^{\#6}$	2.4143(19)
Pr(3)–O(20)	2.4176(19)	Pr(3)–O(34)$^{\#7}$	2.419(2)
Pr(3)–O(1)	2.4831(19)	Pr(3)–O(3*w*)	2.512(2)
Pr(3)–O(14)	2.572(2)	Pr(3)–O(13)	2.703(2)
Pr(3)–O(11)$^{\#5}$	2.944(2)	Pr(4)–O(8)	2.328(2)
Pr(4)–O(32)$^{\#8}$	2.3863(19)	Pr(4)–O(22)$^{\#1}$	2.402(2)
Pr(4)–O(26)	2.4211(19)	Pr(4)–O(4*w*)	2.493(3)
Pr(4)–O(28)$^{\#9}$	2.532(2)	Pr(4)–O(9)$^{\#10}$	2.532(2)
Pr(4)–O(10)$^{\#10}$	2.731(2)		
		II	
Gd(1)–O(1)	2.299(2)	Gd(1)–O(2)$^{\#1}$	2.3165(18)
Gd(1)–O(2*w*)	2.399(2)	Gd(1)–O(8)$^{\#2}$	2.406(2)
Gd(1)–O(1*w*)	2.4572(19)	Gd(1)–O(4)$^{\#3}$	2.4674(18)
Gd(1)–O(7)	2.479(2)	Gd(1)–O(3)$^{\#3}$	2.5392(19)
Gd(1)–O(8)	2.810(3)		

* Symmetry codes: $^{\#1}$ $-x+2, -y+1, -z+1$; $^{\#2}$ $-x+1, -y+1, -z$; $^{\#3}$ $-x+1, -y, -z+1$; $^{\#4}$ $x-1, y-1, z$; $^{\#5}$ $-x+2, -y+1, -z$; $^{\#6}$ $x+1, y, z$; $^{\#7}$ $-x+2, -y, -z+1$; $^{\#8}$ $x, y+1, z$; $^{\#9}$ $x-1, y, z$; $^{\#10}$ $-x+1, -y+2, -z$ (for **I**); $^{\#1}$ $x, -y+3/2, z-1/2$; $^{\#2}$ $-x+1, -y+2, -z$; $^{\#3}$ $-x, -y+2, -z$ (for **II**).

RESULTS AND DISCUSSION

Hydro/solvothermal synthesis has been widely employed to produce functional materials with diverse architectures although the mechanism is not completely clear so far. This method can minimize the problems associated with ligand solubility and enhance the reactivity of reactants. Notably, such a complicated process is often attended by some in situ organic reactions including ligand oxidative coupling, hydrolysis, and substitution [16, 17]. In this work, HFA (formic acid) molecules from the hydrolysis of DMF were observed in the formation of **II**. From a chemical viewpoint, DMF hydrolysis is far from straightforward, however, this has been detected in some examples for anionic coordination networks with the $NH_2Me_2^+$ template [18], or formate ions acting as a participant in the coordination framework [19], as observed in **II**.

Complexes **I**, **II** are all air stable. All general characterizations were carried out on the basis of the crystal samples. The elemental analyses show that the components of these complexes are well consistent with the results of the structural analysis of **I**, **II**. In general, the IR spectra show typical features attributable to each component of the complexes [20]. For example, the IR bands appeared at 1618–1541 and 1465–1379 cm^{-1} can be assigned to the characteristic antisymmetric and symmetric stretching vibrations of carboxylate groups, in consistent with previous publication [7, 11, 20, 21].

Based on crystal structure analyses, four coordination modes were concluded for dicarboxylate in complexes **I**, **II** (Scheme 1): bridging-chelating/bridging (a); bis-bridging (b); bridging-chelating/bridging-monodentate (c); chelating-bridging (d):

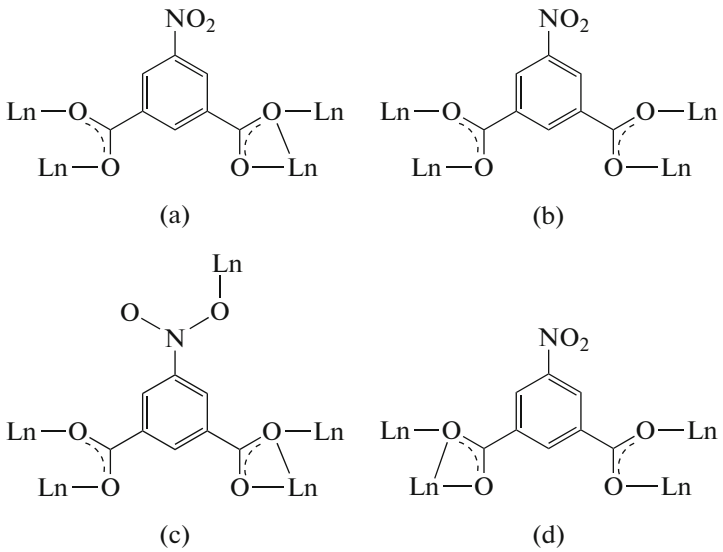

Scheme 1.

Complex **I** exhibits a 3D framework. As shown in Fig. 1a, each asymmetric unit of I contains four Pr^{3+} ions, six L ligands, four coordinated water molecules and two free water molecules. In other words, Pr(1) ion is eight-coordinated by four carboxylate O atoms from three L ligands in the bridging-chelating/bridging coordination mode (Scheme 1a) (Pr(1)–O(25) 2.379(2); Pr(1)–O(13) 2.446(2); Pr(1)–O(2) 2.599(3); Pr(1)–O(1) 2.631(2) Å), two carboxylate O atoms from two L ligands in the bis-bridging coordination mode (Scheme 1b) (Pr(1)–O(21*C*) 2.407(3); Pr(1)–O(19) 2.457(3) Å: $C = -x + 2, -y + 1, -z + 1$), one carboxylate O atom from one L ligand in the bridging-chelating/bridging-monodentate coordination mode (Scheme 1c) (Pr(1)–O(7) 2.393(3) Å) and one O atom from a coordinated water molecule (Pr(1)–O(1*w*) 2.497(3) Å) (Table 2). And Pr(2) ion is coordinated to four carboxylate O atoms from three L ligands in the bridging-chelating/bridging coordination mode (Scheme 1a) (Pr(2)–O(3) 2.418(2); Pr(2)–O(16*D*) 2.350(3); Pr(2)–O(27*F*) 2.573(3); Pr(2)–O(28*F*) 2.715(2) Å; $D = -x + 1, -y + 1, -z$; $F = x - 1, y - 1, z$), two carboxylate O atoms from two L ligands in the bis-bridging coordination mode (Scheme 1b) (Pr(2)–O(31) 2.440(3); Pr(2)–O(33*E*) 2.372(3) Å; $E = -x + 1, -y, -z + 1$), one carboxylate O atom from one L ligand in the bridging-chelating/bridging-monodentate coordination mode (Scheme 1c) (Pr(2)–O(10*D*) 2.466(2) Å; $D = -x + 1, -y + 1, -z$) and one O atom from a coordinated water molecule (Pr(2)–O(2*w*) 2.536(3) Å) (Table 2). While Pr(3) ion is nine-coordinated by five carboxylate O atoms from four L ligands in the bridging-chelating/bridging coordination mode (Scheme 1a) (Pr(3)–O(1) 2.483(2); Pr(3)–O(4*H*) 2.413(2); Pr(3)–O(14) 2.571(3); Pr(3)–O(13) 2.704(3); Pr(3)–O(15*G*) 2.373(3) Å; $G = -x + 2, -y + 1, -z$; $H = x + 1, y, z$), two carboxylate O atoms from two L ligands in the bis-bridging coordination mode (Scheme 1b) (Pr(3)–O(20) 2.419(3); Pr(3)–O(34*I*) 2.419(3) Å; $I = -x + 2, -y, -z + 1$), one carboxylate O atom from one L ligand in the bridging-chelating/bridging-monodentate coordination mode (Scheme 1c) (Pr(3)–O(11*G*) 2.945(3) Å; $G = -x + 2, -y + 1, -z$) and one O atom from a coordinated water molecule (Pr(3)–O(3*w*) 2.514(3) Å) (Table 2). And Pr(4) ion is coordinated to two carboxylate O atoms from two L ligands in the bridging-chelating/bridging coordination mode (Scheme 1a) (Pr(4)–O(26) 2.418(2); Pr(4)–O(28*K*) 2.532(3) Å; $K = x - 1, y, z$), two carboxylate O atoms from two L ligands in the bis-bridging coordination mode (Scheme 1b) (Pr(4)–O(32*J*) 2.386(2); Pr(4)–O(22*C*) 2.402(3) Å; (C) $= -x + 2, -y + 1, -z + 1$; (J) $= x, y + 1, z$), three carboxylate O atoms from two L ligands in the bridging-chelating/bridging-monodentate coordination mode (Scheme 1c) (Pr(4)–O(8) 2.328(3); Pr(4)–O(9*L*) 2.532(3); Pr(4)–O(10*L*) 2.731(3) Å; $L = -x + 1, -y + 2, -z$) and one O atom from a coordinated water moleculeand one O atom from a coordinated water molecule (Pr(4)–O(4*w*) 2.493(3) Å) (Table 2). All Pr–O bond distances and OPrO angles are all within the range observed for other Pr(III) complexes [22]. The four Pr^{3+} ions are connected to adjacent Pr^{3+} ions through L ligands to result in a 3D framework. The open space (void volume = 219.2 $Å^3$, 7.2% of the unit cell volume) still exists within the coordination network of **I**.

The dinuclear of Pr(1) and Pr(3) as well as that of Pr(2) and Pr(4) can be regarded as a nine-connecting node, while the L ligand acts as topologically three- or four-connecting to bridge adjacent dinuclear units. This leads to a 3D topology network (Fig. 1b) with a Schläfli symbol of $\{4.6^2\}\{4^{10}.6^{17}.8^9\}\{4^3\}_2$.

(a)

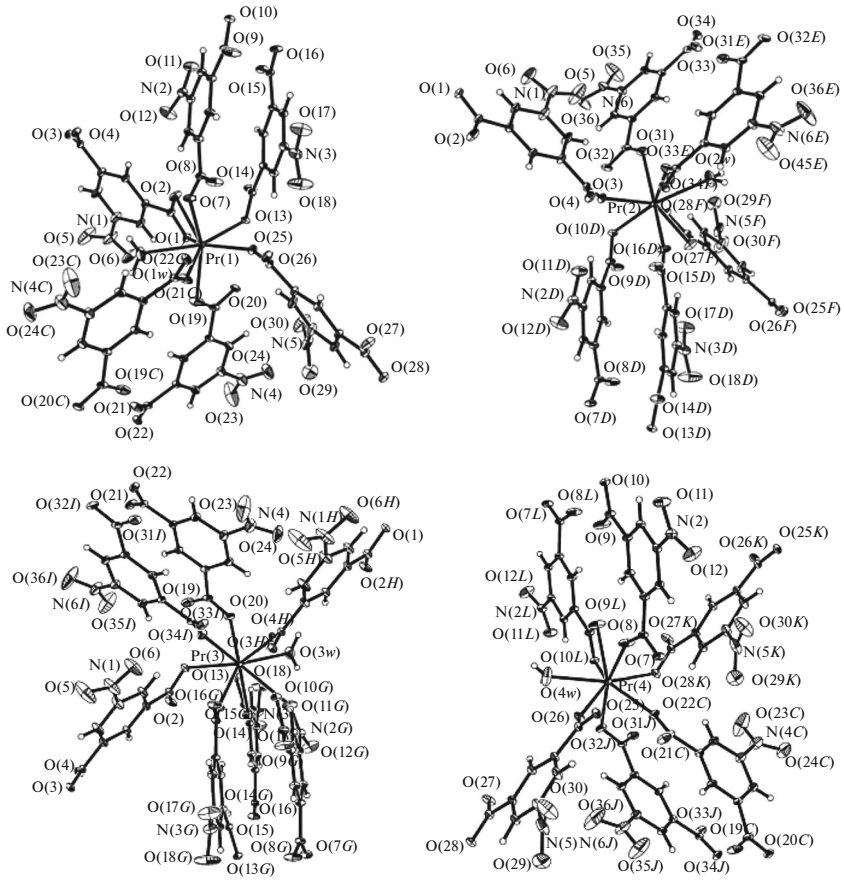

(b)

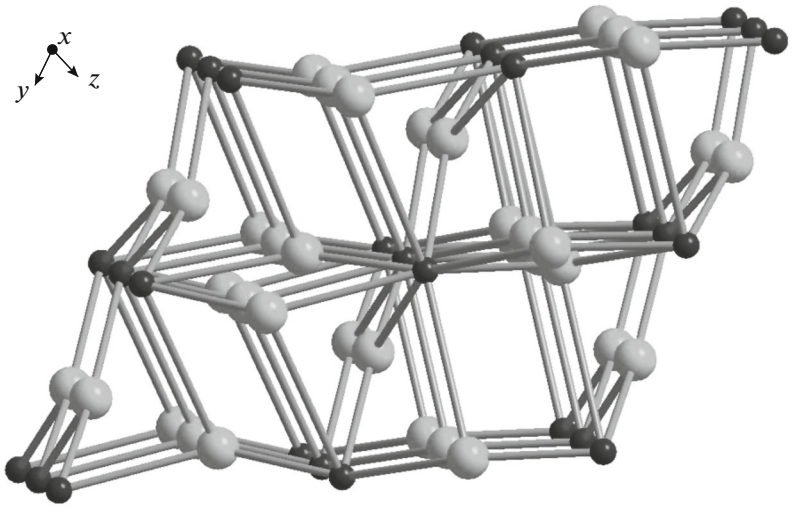

Fig. 1. View of coordination environment of Pr(1), Pr(2), Pr(3) and Pr(4) in **I** with 30% probability ellipsoid (a); schematic representations of a 3D $\{4.6^2\}\{4^{10}.6^{17}.8^9\}\{4^3\}_2$ topology framework in **I** (free aqua molecules omitted for clarity) (b). Symmetry codes: $C = -x + 2, -y + 1, -z + 1$; $D = -x + 1, -y + 1, -z$; $E = -x + 1, -y, -z + 1$; $F = x - 1, y - 1, z$; $G = -x + 2, -y + 1, -z$; $H = x + 1, y, z$; $I = -x + 2, -y, -z + 1$; $J = x, y + 1, z$; $K = x - 1, y, z$; $L = -x + 1, -y + 2, -z$.

(a)

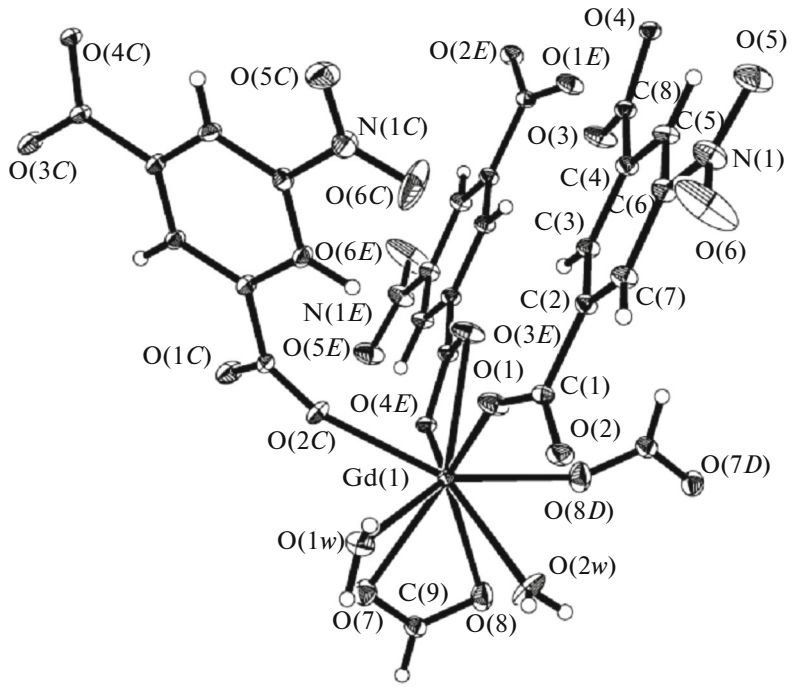

(b)

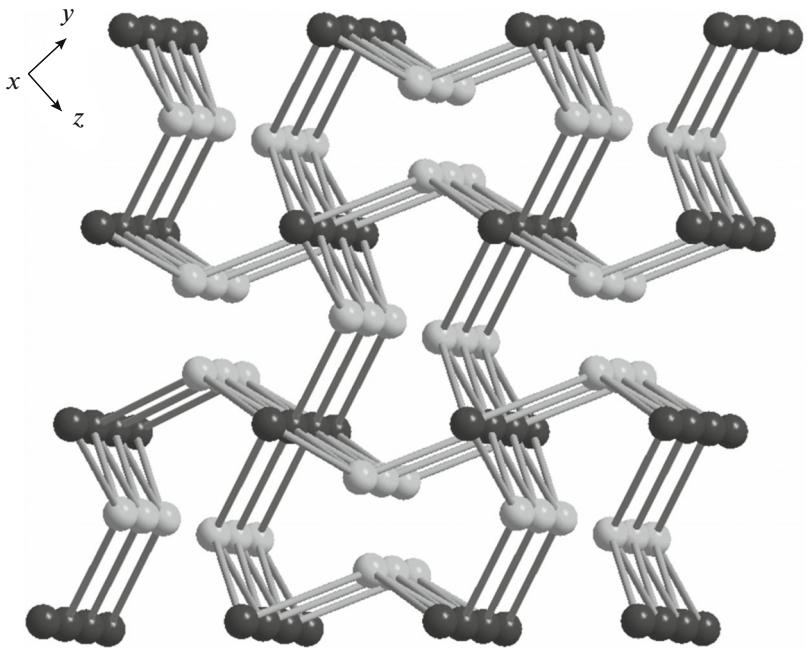

Fig. 2. View of coordination environment of Gd(III) in **II** with 30% probability ellipsoid (a); schematic representations of a 3D $\{4.6^2\}_2\{4^2.6^{10}.8^3\}$ topology framework in **II** (b). Symmetry codes: $C = x, -y + 3/2, z - 1/2$; $D = -x + 1, -y + 2, -z$; $E = -x, -y + 2, -z$.

When solvent DMF was introduced into the synthetic conditions, a distinct 3D network from complex **I** is produced for complex **II**. The asymmetric unit of **II** is composed of one Gd^{3+} ion, one L ligand, one FA ligand from the hydrolysis of DMF and two coordinated water molecules. As shown in Fig. 2a, each Gd(III) center is nine-coordinated by four carboxylate O atoms from three different L ligands in the chelat-

ing-bridging coordination mode (Scheme 1d), one FA ligand in the bridging coordination mode and one FA ligand in the chelating/bridging coordination mode, and two O atoms from two coordinated water molecules with Gd–O bond lengths ranging from 2.299(2) to 2.810(3) Å (Table 2) and OGdO bond angles ranging from 47.94(6)° to 147.12(7)° [22]. The Gd^{3+} ion is connected to an adjacent Gd^{3+} ion through two FA ligands to result in a dinuclear $[Gd_2(FA)_2(H_2O)_4]$ unit, which is further connected to adjacent dinuclear units through L ligands to result in a 3D framework.

Simplying the dinuclear $[Gd_2(FA)_2(H_2O)_4]$ unit as a six-connecting node, which is bridged with adjacent dinuclear nodes by the three-connecting L ligands, results in a 3D topology framework for complex **II** with a Schläfli symbol of $\{4.6^2\}_2\{4^2.6^{10}.8^3\}$ (Fig. 2b).

In the previously publications [11, 21, 23–30], H_2P (phthalic acid), H_2Tp (terephthalic acid), H_2Ip (isophthalic acid) and H_2(HO-Ip) (hydroxyisophthalic acid) liagnds were used to construct a 2D corrugated sheet $Ln_2[(P)_3]_n$ (Ln = Gd) [23], a ladder-like arrangement 3D framework with rhombic one-dimensional channels $[Ln_2(H_2O)_4(P)_2(Tp)]_n$ (Ln = Pr) [24], a corrugated step-like ladder arrangement 3D framework $[Ln_2(H_2O)_4(P)_2(Tp)]_n$ (Ln = Gd) [24], a 3D framework with an interconnectivity chainlike arrangement $[Ln_2(Tp)_2(NO_3)_2(DMF)_4]_n$ (Ln = Gd) [25], isostructural 2D networks of $[Ln_2(Ip)_3(H_2O)_2]_n$ (Ln = Pr or Gd) [26], a 3D framework with right-handed helices $[Ln_2(HO\text{-}Ip)_3(H_2O)_2]_n$ (Ln = Pr) [27] and a 1D zigzag chain $\{[Ln_2(HO\text{-}Ip)_2](HO\text{-}Ip)(H_2O)_2\}_n$ (Ln = Gd) [28]. In this research, replacing H_2Ip with H_2L, a 3D $\{4.6^2\}\{4^{10}.6^{17}.8^9\}\{4^3\}_2$ topology framework for **I** (Ln = Pr) was obtained. While solvent DMF molecules were introduced into the synthetic condition, HFA molecules from the hydrolysis of DMF were observed, similar to the previously publications the 3D pillar-layer network $[Ln(Tp)(FA)]_n$ (Ln = Gd) [29]. And a 3D $\{4.6^2\}_2\{4^2.6^{10}.8^3\}$ topology network for **II** (Ln = Gd) was produced.

This work gives a good comparison between different backbone carboxylate complexes. The results indicate that ligand backbone has vital influence to the architecture of target MOFs, meanwhile, solvents used also have deep influence to the final structure, which may play an important role in the luminescent properties.

To confirm whether the crystal structures are truly representative of the bulk materials, XRPD experiments have also been carried out for **I**, **II**. In comparison with those simulated from crystal modes, the bulk-synthesized materials and as-grown crystals can be considered homogeneous for **I**, **II**.

The luminescence of **I**, **II** as well as free ligands H_2L were investigated in the solid state at room temperature (Fig. 3). For free ligands H_2L, the emission

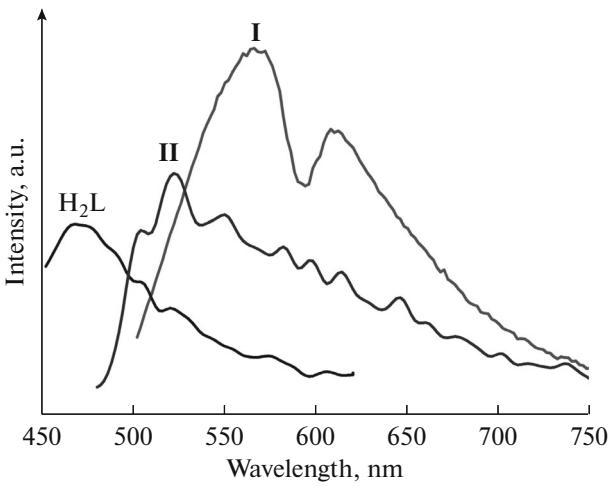

Fig. 3. Emission spectra of **I**, **II** and ligand H_2L in the solid state at room temperature (λ_{ex} = 499 nm for **I**, 344 nm for **II** and 430 nm for H_2L).

peak was observed at 477 nm (λ_{ex} = 430 nm). It is clear that there are two emission peaks at 565/609 nm for **I** (λ_{ex} = 499 nm) and one emission peak at 519 nm for **II** (λ_{ex} = 344 nm), respectively.

According to the reported results on coordination polymers with benzene backbone [5], the observed emissions were generally attributed to intraligand π*–π transitions, namely, ligand-to-ligand charge transfer (LLCT). In **I** and **II**, a red-shift phenomenon was observed compared with the emission of H_2L, due to the deprotonation of the ligands when forming the 3D network. We believe that the π···π stacking interactions between ligands may also lead to the red-shift phenomenon [31]. Moreover, the different relative intensity among **I**, **II** might be assigned to the structural diversity along with a different ratio of H_2L ligands [32].

In addition, it's worth noticing that because of no antenna effect [33], no obvious emission attributable to rare earth ion was observed for complexes **I**, **II**, differing from the previously reported lanthanide luminescence [34].

Two Ln(III) MOFs with 5-nitroisophthalic acid have been synthesized and characterized. The study of the synthesis and structures of the complexes validate the vital effect of ligand backbone, on the final MOFs architecture. Because of the in situ hydrolysis of DMF solvates, formate ions were observed in the structure of **II**. In addition, luminescent properties of complexes **I**, **II** in the solid state at room temperature were attributed to the LLCT of corresponding ligands.

ACKNOWLEDGMENTS

This work was supported by NSFC (no. 21403006), the key project of Science, the Technology Depart-

ment of Henan province (no. 112102210371) and the science and technology research projects of Education Department of Henan province (no. 12B150003).

REFERENCES

1. Tian, D., Chen, Q., Li, Y., et al., *Angew. Chem. Int. Ed.*, 2014, vol. 53, p. 837.
2. Cheng, X.N., Xue, W., Lin, J.B., et al., *Chem. Commun.*, 2010, vol. 46, p. 246.
3. Du, M., Li, C.P., Chen, M., et al., *J. Am. Chem. Soc.*, 2014, vol. 136, p. 10906.
4. Li, Y.W., Ma, H., Chen, Y.Q., et al., *Cryst. Growth Des.*, 2012, vol. 12, p. 189.
5. Sakata, Y., Furukawa, S., Kondo, M., et al., *Science*, 2013, vol. 339, p. 193.
6. Gong, H.Y., Rambo, B.M., Karnas, E., et al., *J. Am. Chem. Soc.*, 2011, vol. 133, p. 1526.
7. Hirai, K., Furukawa, S., Kondo, M., et al., *Angew. Chem. Int. Ed.*, 2011, vol. 50, p. 8057.
8. Jarikov, V.V. and Kondakov, D.Y., *J. Appl. Phys.*, 2009, vol. 105, p. 034905.
9. Ghosh, S., Chakrabarty, R., and Mukherjee, P.S., *Inorg. Chem.*, 2009, vol. 48, p. 549.
10. Terazono, Y., Kodis, G., Liddell, P.A., et al., *J. Phys. Chem., B*, 2009, vol. 113, p. 7147.
11. Gao, J.Y., Xiong, X.H., Chen, C.J., et al., *Inorg. Chem. Commun.*, 2013, vol. 31, p. 5.
12. *SAINT, Software Reference Manual*, Madison: Bruker, AXS, 1998.
13. Sheldrick, G.M., *SADABS, Siemens Area Detector Absorption Corrected Software*, Göttingen: Univ. of Göttingen, 1996.
14. Sheldrick, G.M., *SHELXTL NT, Version 5.1, Program for Solution and Refinement of Crystal Structures*, Göttingen: Univ. of Göttingen, 1997.
15. Paul, M., Adarsh, N.N., and Dastidar, P., *Cryst. Growth Des.*, 2014, vol. 14.
16. Zhang, J.P., Zheng, S.L., Huang, X.C., et al., *Angew. Chem. Int. Ed.*, 2004, vol. 43, p. 206.
17. Wang, D. and Astruc, D., *Chem. Rev.*, 2014, vol. 114, p. 6949.
18. Xue, Y.S., Jin, F.Y., Zhou, L., et al., *Cryst. Growth Des.*, 2012, vol. 12, p. 6158.
19. Wang, C., Wang, J.L., and Lin, W., *J. Am. Chem. Soc.*, 2012, vol. 134, p. 19895.
20. Nakamoto, K., *Infrared and Raman Spectra of Inorganic and Coordination Compounds*, New York: Wiley, 1986.
21. Zhang, G., Zhao, X., Dai, F., et al., *Inorg. Chem. Commun.*, 2011, vol. 14, p. 948.
22. Taylor, J.M., Dawson, K.W., and Shimizu, G.K.H., *J. Am. Chem. Soc.*, 2013, vol. 135, p. 1193.
23. Meng, Z.R., Zhang, Q.Z., Wu, X.Y., et al., *Acta Crystallogr., Sect. E: Struct. Rep. Online*, 2006, vol. 62, p. m1033.
24. Thirumurugan, A. and Natarajan, S., *Eur. J. Inorg. Chem.*, 2004, p. 762.
25. Liao, L., Ingram, C.W., Vandeveer, D., et al., *Inorg. Chim. Acta*, 2012, vol. 391, p. 1.
26. Fu, F., Chen, S.P., Ren, Y.X., et al., *Acta Chim. Sin.*, 2008, vol. 66, p. 1663.
27. Lin, L., Zhang, X., Zhang, J., et al., *J. Mol. Struct.*, 2011, vol. 1006, p. 83.
28. Xu, H. and Li, Y., *J. Mol. Struct.*, 2004, vol. 690, p. 137.
29. Sibille, R., Mazet, T., Malaman, B., et al., *Chem. Eur. J.*, 2012, vol. 18, p. 12970.
30. Fang, X., Cai, L.M., Shao, Y.C., et al., *J. Coord. Chem.*, 2014, vol. 67, p. 3542.
31. Carrera, E.I., McCormick, T.M., Kapp, M.J., et al., *Inorg. Chem.*, 2013, vol. 52, p. 13779.
32. Chang, Z., Zhang, A.S., Hu, T.L., et al., *Cryst. Growth Des.*, 2009, vol. 9, p. 4840.
33. Allendorf, M.D., Bauer, C.A., Bhakta, R.K., et al., *Chem. Soc. Rev.*, 2009, vol. 38, p. 1330.
34. Zhou, R.S., Cui, X.B., Song, J.F., et al., *J. Solid State Chem.*, 2008, vol. 181, p. 2099.